Supplementary Material, Part-2:

Chlorocobalt(II) complexes with pyridylethyl-derived diazacycloalkanes.

Anthony W. Addison,[a]* Stephen J. Jaworski,[a†] Jerry P. Jasinski,[b‡] Elizabeth A. Brayman,[a†] Mark M. Turnbull,[c] Fan Xiao,[c] Matthias Zeller[d] & Molly A. O'Connor.[a]

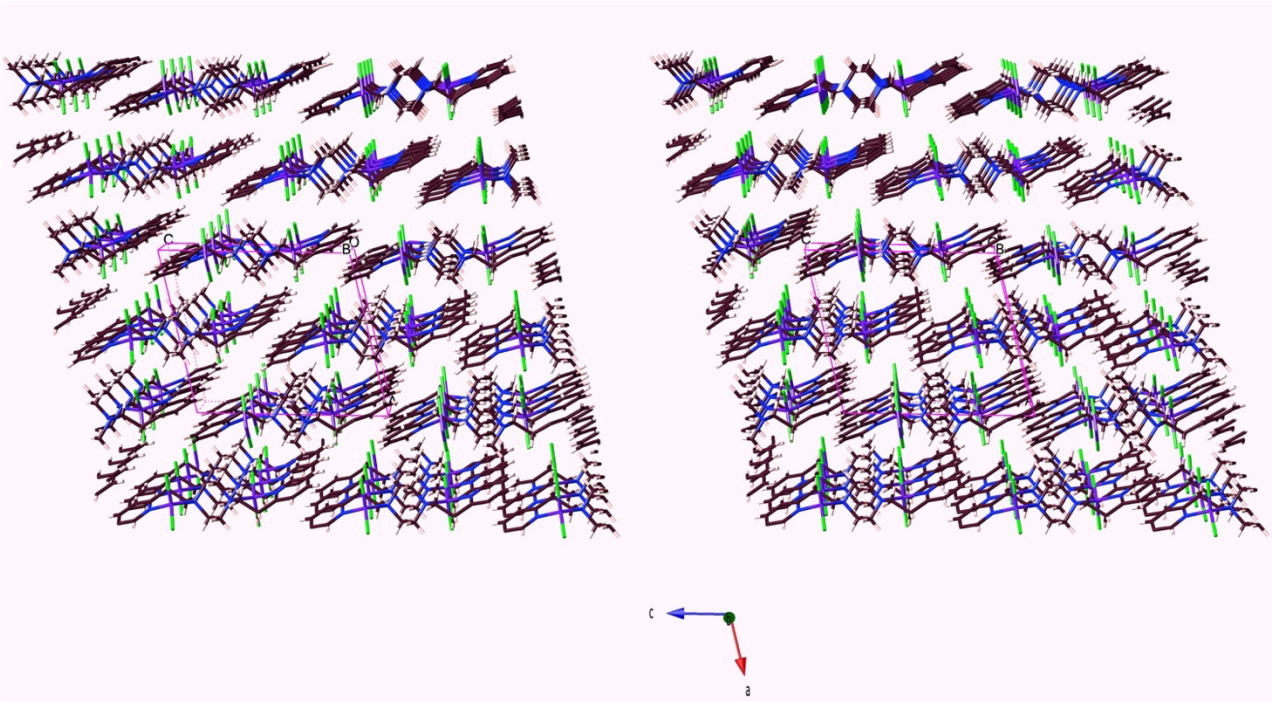

Fig. S1: Lattice fragment stick diagram of $Co_2(Ppz)Cl_4$: inverse stereoview along the *b*-direction, showing interdigitation of the dinuclear molecules.

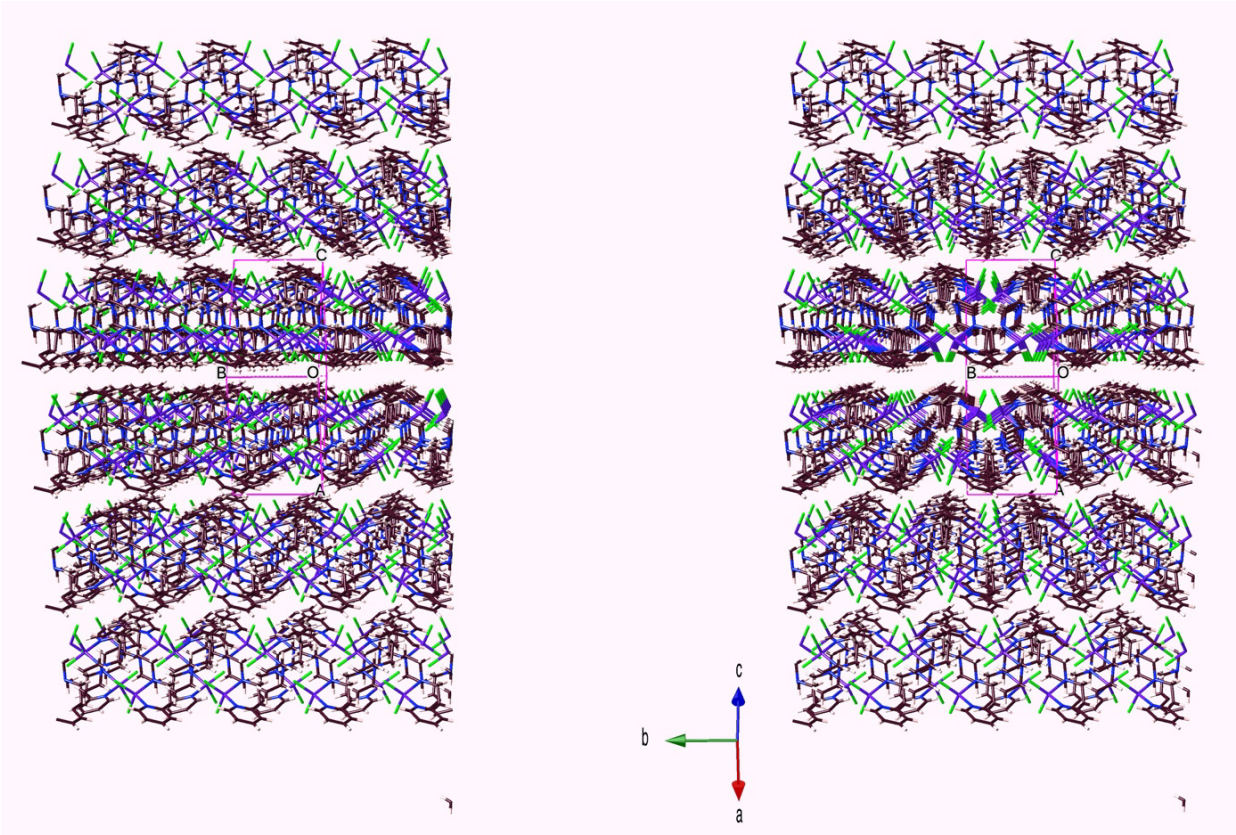

Fig. S2: Inverse stereoview of the $Co_2(Ppz)Cl_4$ lattice along a direction between the *a*- and *c*-axes, showing its double layers of molecules.

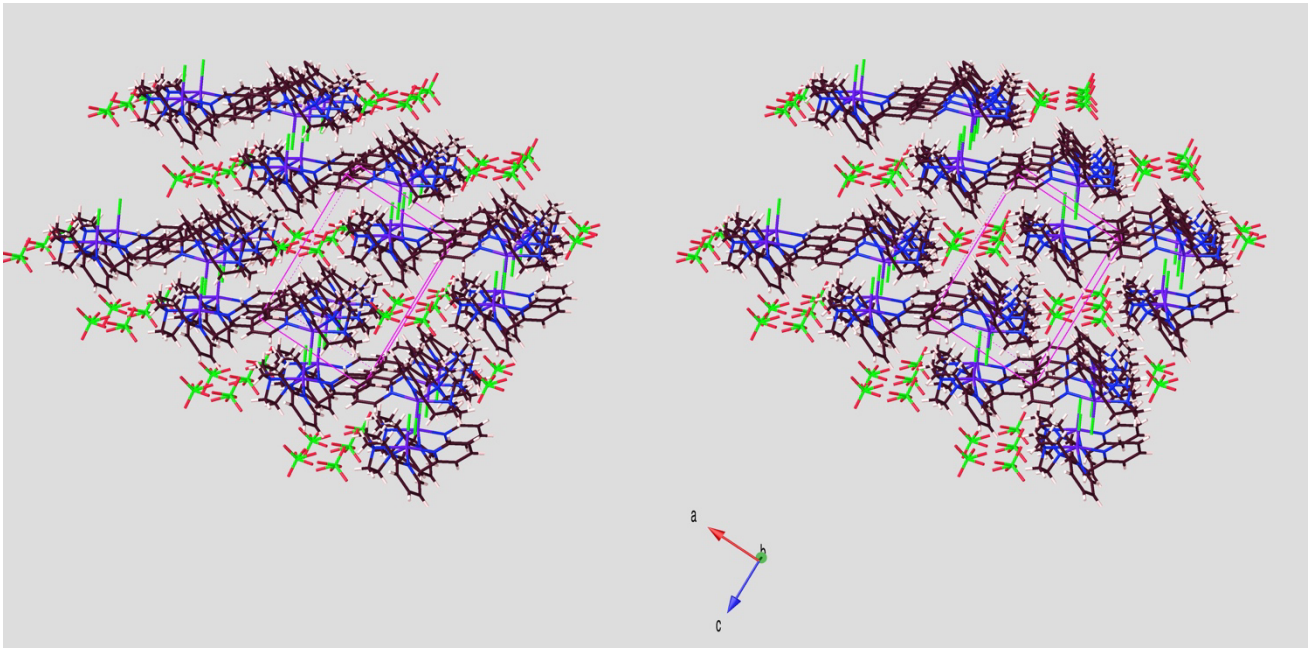

Fig. S3: Inverse stereoview of the [Co(Ppz)Cl]ClO_4 lattice along the *b*-axis, showing interdigitation of the cation layers and *b*-stacking of the perchlorates.

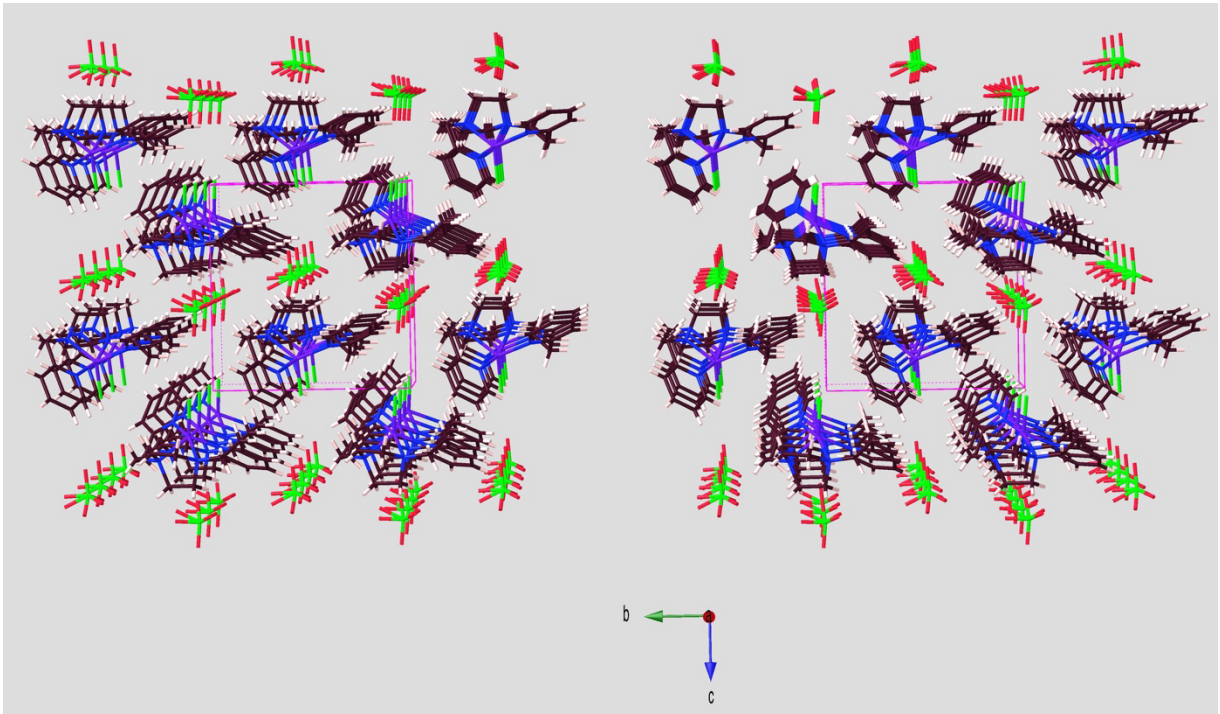

Fig. S4: Inverse stereoview of the [Co(Ppz)Cl]ClO_4 lattice along the *a*-direction, showing stacked arraying of the cations and perchlorates.

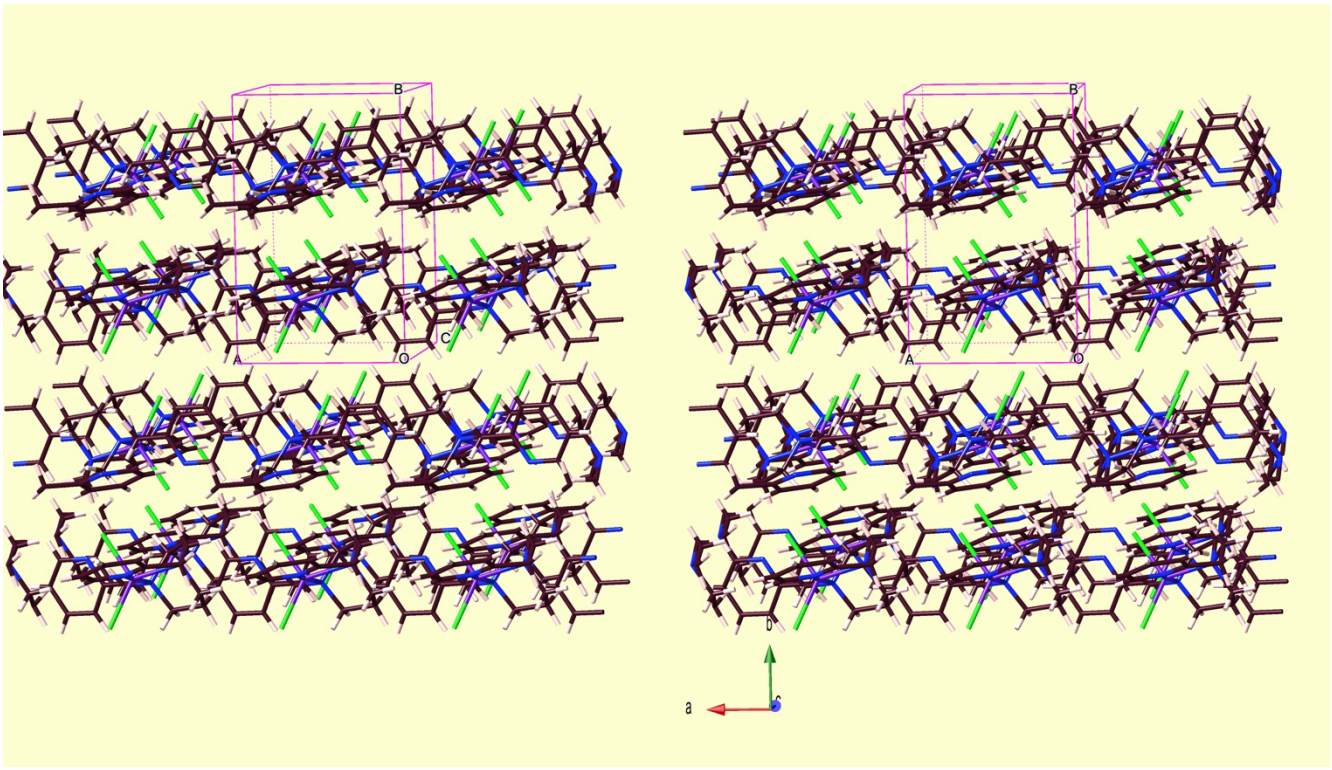

Fig. S5: Inverse stereoview of the Co(Phpz)Cl_2 lattice obliquely along the *c*-axis, showing *b*-direction layering of the molecules.

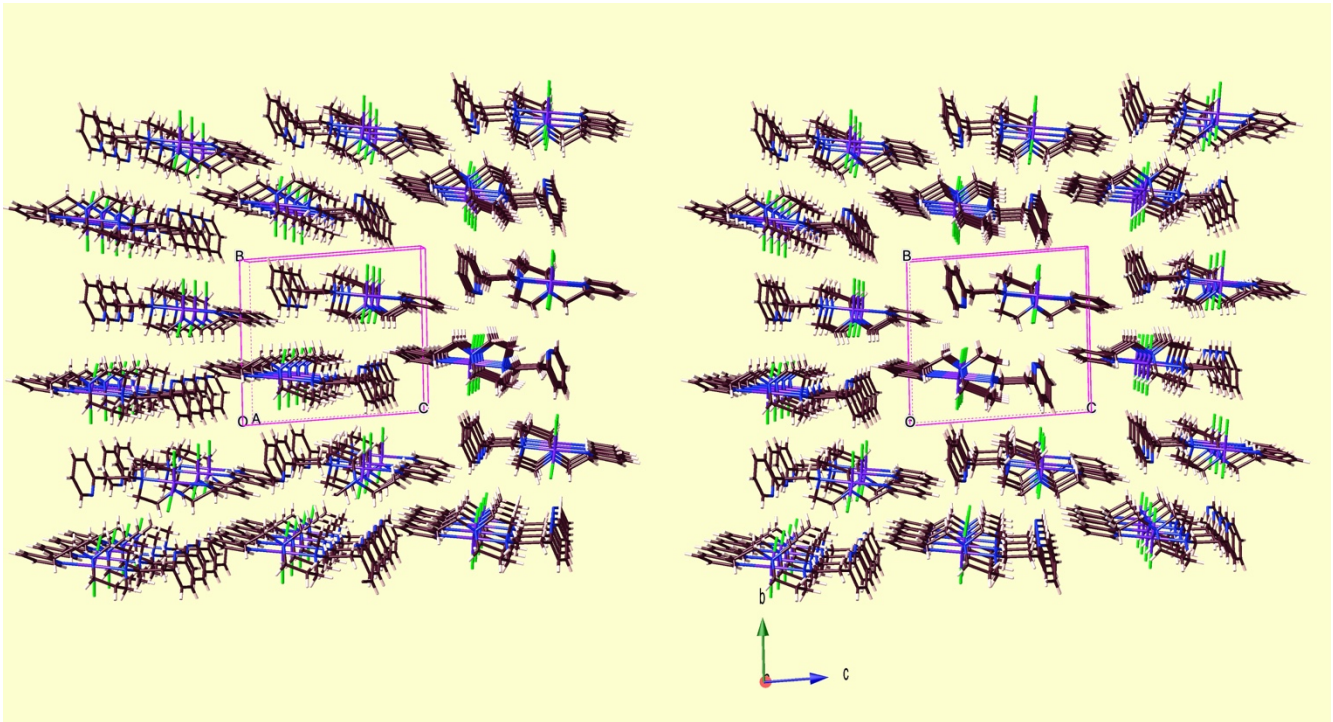

Fig. S6: Inverse stereoview of the Co(Phpz)Cl_2 lattice obliquely along the *a*-direction, showing *a*-direction arraying and slipped layering of the molecules.

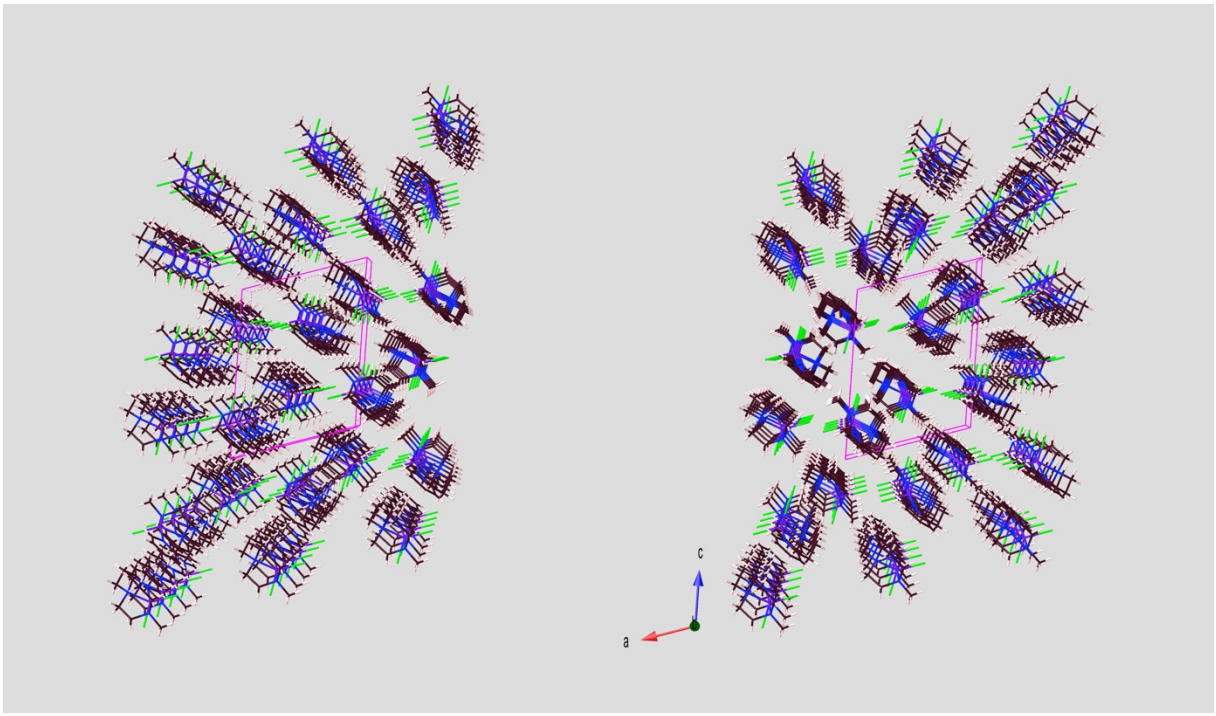

Fig. S7: Inverse stereoview of the Co(Pmhpz)Cl_2 lattice along the *b*-direction arraying of the molecules. , showing *b*-direction layering of the molecules.

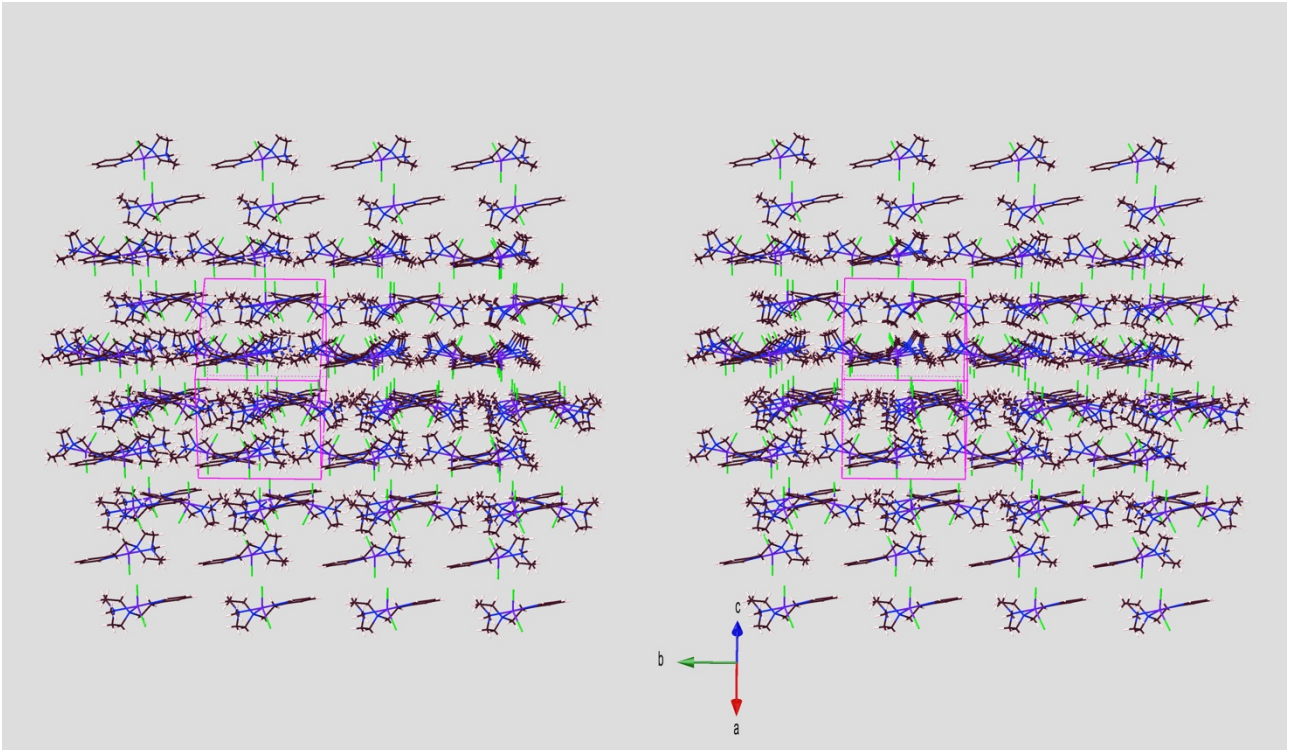

Fig. S8: Inverse stereoview of the Co(Pmhpz)Cl_2 lattice along a direction between the *a*- and *c*-axes, showing layering of the molecules.

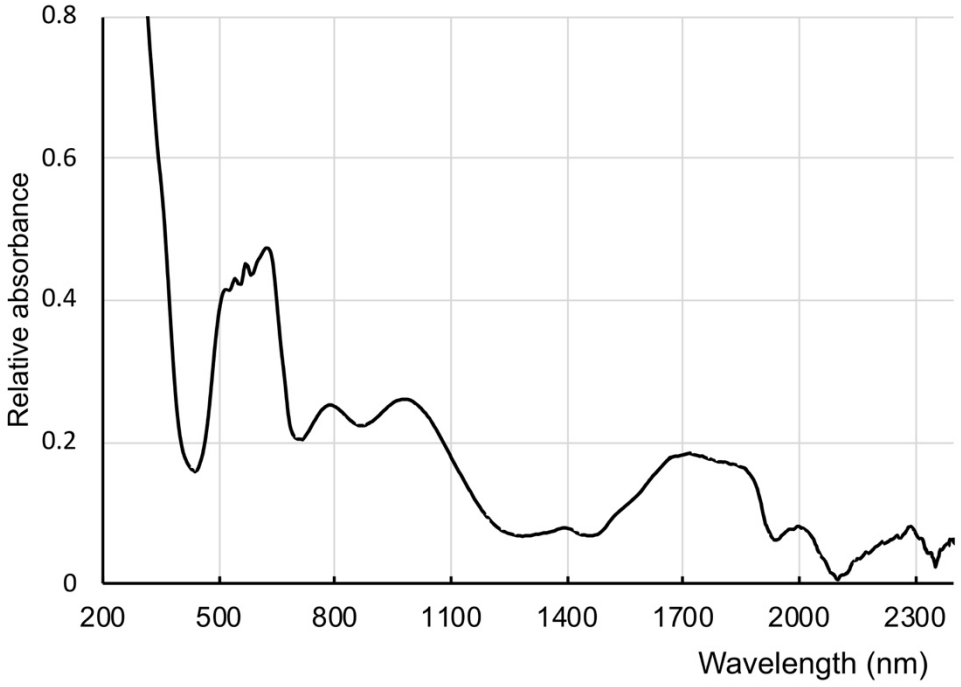

Fig. S9: Solid-state Vis-NIR reflectance spectrum of Co(Pmhpz)Cl_2.

Table S1: Some examples of electronic spectra for tetra- and pentacoordinate Co(II) complexes.

Notes	Reference	
Tetra- & pentacoordinate, Vis-NIR used.	1965	Goodgame
Some NIR, fully not utilised	1971	Latt
Tetracoordinate, NIR	1992	Trofimenko
Tetra- & pentacoordinate, visible region only.	1993	Han
Visible region only, for tetragonal-pyramidal	1997	Kremer-Ach
Pentacoordinate, no electronic spectra.	1998	Boca
Octahedral, Vis-NIR.	2004	Chandra
Tetrahedral, visible region only.	2005	Stanescu
Pentacoordinate, visible region only.	2009	Sabiah
NIR for tetracoordinate	2010	Krzystek
Vis-NIR for tetragonal-pyramidal	2012	Kochem
Tetra- & pentacoordinate, visible region only.	2014	Ward
Pentacoordinate, no electronic spectra.	2018	Sadhu
NIR of Co(III) only	2020	Kanso

1965: Goodgame, D.M.L. & Goodgame, M. (1965) *Inorg. Chem*. **4**, 139-143.
1971: Latt, S.A. & Vallee, B.L. (1971) *Biochem*. **10**, 4263-4270.
1992: Trofimenko, S., Calabrese, J.C., Kochi, J.K., Wolowiec, S., Hulsbergen, F.B. & Reedijk, J. (1992) *Inorg. Chem.* **31**, 3943-3950.
1993: Han, H., Looney, A., McNeill, K., Parkin, G., Rheingold, A.L. & Haggerty, B.S. (1993) *J.*

Inorg. Biochem. **49**, 105-121.
1997: Kremer-Ach, A., Kläui, W., Bell, R., Strerath, A. Wunderlich, H. & Mootz, D. (1997) *Inorg. Chem.*, **36**, 1552-1563.
1998: Boca, R., Elias, H., Haase, W., Hüber, M., Klement, R., Müller, L., Paulus, H., Svoboda, I. & Valko, M. (1998) *Inorg. Chim. Acta*. **278**, 127-135.
2004: Chandra, S. & Gupta, L.K. (2004) *Spectrochim. Acta* **60**, 3079-3085.
2005: Stanescu,G. & Trutia, A. (2005) *J. Optoelect. Adv. Mat*., **7**, 1009-1015
2009: Sabiah, S., Varghese, B. & Murthy, N.N. (2009) *Dalton Trans*. 9770-9780.
2010: Krzystek, J., Swenson, D.C., Zvyagin, S.A., Smimov, D., Ozarowski, A. & Telser, J. (2010) *J.Am.Chem.Soc.* **132**, 5241-5253.
2012: Kochem, A., Kanso, H., Baptiste, B., Arora, H., Philouze, C., Jarjayes, O., Vezin, H., Luneau, D., Orio, M. & Thomas, F. (2012) *Inorg. Chem*. **51**, 10557-10571.
2014: Ward, A.L., Lukens, W.W., Lu, C.C. & Arnold, J. (2014) *J.Am.Chem.Soc.* **136**, 3647-3653.
2018: Sadhu, M.H. & Kumar, S.B. (2018) *J.Mol. Struct.* **1164**, 239-247.
2020: Kanso, H., Clarke, R.M., Kochem, A., Arora, H., Philouze, C., Jarjayes, O., Storr, T. & Thomas, F. (2020) *Inorg. Chem.* **59**, 5133-5148.

Magnetism background:

For interpretation of the magnetic data, a simple and effective model was employed, using the Hamiltonian: $\boldsymbol{H} = DS_z^2 + h \cdot S$

where D is the axial single ion anisotropy (SIA) term and h is the external field. The rhombic SIA term (E) is neglected as its effect is suppressed in powder measurements. No inter-molecule coupling (zJ) is taken into account, as indicated above; in any case, such would be very small compared with D.

One might note, that a single g-value (g_{ave}) is used here for the calculation of the isotropic susceptibilities χ_x^{ISO} and χ_z^{ISO}. The differences between the g-tensor along the two axes are incorporated into the term Δ. The presence of D splits the $|\pm 1/2\rangle$ and $|\pm 3/2\rangle$ Kramers doublets and introduces an energy gap of $4D$, causing the magnetism to deviate from the simple paramagnetic state (S=3/2 for high-spin Co^{2+}) at low temperature. A positive D-value lowers the $|\pm 1/2\rangle$ doublet energy, favoring the XY-like spin, while negative D lowers the energy of the $|\pm 3/2\rangle$ doublet, yielding a more Ising-like behaviour. The sign of D also has an impact on the spin anisotropy.

The individual products of molar susceptibility and temperature ($\chi_x T$ and $\chi_z T$) can be derived using the exact diagonalization of the spin Hamiltonian for both longitudinal ($h//z$) and transverse ($h//x$) modes. The powder average then takes the simple form of:

$$\chi T = \frac{2}{3}\chi_x T + \frac{1}{3}\chi_z T$$

In practice, we have rewritten the formula to account for the anisotropic ($\Delta = S_x/S_z$) responses as well as the linear TIP contribution to χ (typically 400-800x10^{-6} cgsu for $^4A_2$ ground state Co^{2+}; (Earnshaw, 1968) and ligands' diamagnetic contribution, respectively ($aT+b$):

$$\chi T = \frac{2\Delta}{2\Delta + 1}\chi_x^* T + \frac{1}{2\Delta + 1}\chi_z^* T + aT + b$$

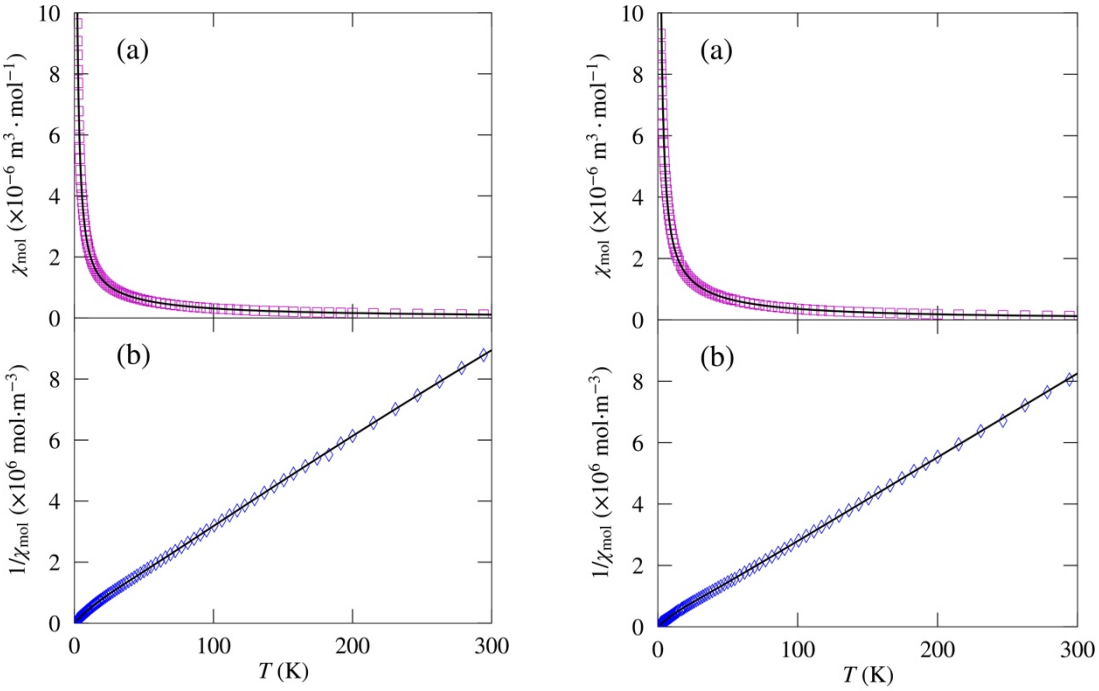

Figure S10:
Left half: for $Co(Phpz)Cl_2$ - (a) temperature dependence of the molar susceptibility χ_M (H=0.1 T). Open symbols are the experimental data and the solid line represents the fit; (b) temperature dependence of the inverse molar susceptibility, $1/\chi_M$ (H=0.1 T).
Right half: (a) temperature dependence of the molar susceptibility χ_M of $Co(Pmhpz)Cl_2$ (H=0.1 T). Open symbols are the experimental data and the solid line represents the fit; (b) temperature dependence of the inverse molar susceptibility $1/\chi_M$ (H=0.1 T).

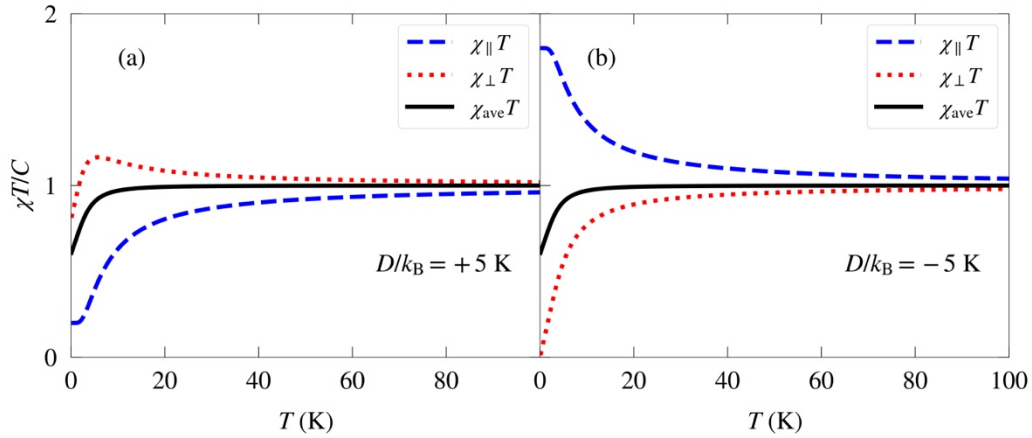

Figure S11: Illustration of the ZFS components and their outcomes.
(a) Longitudinal ($\chi_{\parallel}$), transverse ($\chi_{\perp}$) and powder average susceptibilities of a paramagnetic S=3/2 system with positive D. Longitudinal denotes the orientation parallel to D and transverse denotes the orientation perpendicular to D. χ_{ave} is calculated as $3\chi_{ave} = \chi_{\parallel} + 2\chi_{\perp}$. The ordinate is normalized with respect to the Curie constant.
(b) Longitudinal ($\chi_{\parallel}$), transverse ($\chi_{\perp}$) and powder average susceptibilities of a paramagnetic S=3/2 system with negative D. Same notation as (a).

References:

Earnshaw, A., *Introduction to Magnetochemistry*, Academic Press, London/New York, 1968, pp.67.

Sample codes for cobalt preps.

$[Co_2(Ppz)Cl_4]$ = SJ1501. SJ1505, SJ1507, SJ1622, EAB1604

$[Co(Phpz)Cl_2]$ = SJ1511B, EAB1608, EAB1703, TA1807, TA2104

$[Co(Ppz)Cl](ClO_4)$ = SJ1510, SJ1514, EAB1701C

$[Co(Pmhpz)Cl_2]$ = EAB1607

$[Co(Pdmpz)Cl_2]$ = SJ1515, SJ1622, EAB1607, EAB1609